Published in final edited form as:
Integr Biol (Camb). 2012 October ; 4(10): . doi:10.1039/c2ib20171b.

Advancing practical usage of microtechnology: a study of the functional consequences of dielectrophoresis on neural stem cells

Jente Lu[a,b,*], **Chesca A. Barrios**[b], **Amanda R. Dickson**[b], **Jamison L. Nourse**[b], **Abraham P. Lee**[a], and **Lisa A. Flanagan**[b,*]

[a]Department of Biomedical Engineering, University of California at Irvine, Irvine, CA 92697

[b]Department of Neurology and Sue & Bill Gross Stem Cell Research Center, University of California at Irvine, Irvine, CA 92697

Abstract

The integration of microscale engineering, microfluidics, and AC electrokinetics such as dielectrophoresis has generated novel microsystems that enable quantitative analysis of cellular phenotype, function, and physiology. These systems are increasingly being used to assess diverse cell types, such as stem cells, so it becomes critical to thoroughly evaluate whether the systems themselves impact cell function. For example, engineered microsystems have been utilized to investigate neural stem/progenitor cells (NSPCs), which are of interest due to their potential to treat CNS disease and injury. Analysis by dielectrophoresis (DEP) microsystems determined that unlabeled NSPCs with distinct fate potential have previously unrecognized distinguishing electrophysiological characteristics, suggesting that NSPCs could be isolated by DEP microsystems without the use of cell type specific labels. To gauge the potential impact of DEP sorting on NSPCs, we investigated whether electric field exposure of varying times affected survival, proliferation, or fate potential of NSPCs in suspension. We found short-term DEP exposure (1 min or less) had no effect on NSPC survival, proliferation, or fate potential revealed by differentiation. Moreover, NSPC proliferation (measured by DNA synthesis and cell cycle kinetics) and fate potential were not altered by any length of DEP exposure (up to 30 min). However, lengthy exposure (> 5 min) to frequencies near the crossover frequency (50–100 kHz) led to decreased survival of NSPCs (maximum ~30% cell loss after 30 min). Based on experimental observations and mathematical simulations of cells in suspension, we find that frequencies near the crossover frequency generate an induced transmembrane potential that results in cell swelling and rupture. This is in contrast to the case for adherent cells since negative DEP frequencies lower than the crossover frequency generate the highest induced transmembrane potential and damage for these cells. We clarify contrasting effects of DEP on adherent and suspended cells, which are related to the cell position within the electric field and the strength of the electric field at specific distances from the electrodes. Modeling of electrode configurations predicts optimal designs to induce cell movement by DEP while limiting the induced transmembrane potential. We find DEP electric fields are not harmful to stem cells in suspension at short exposure times, thus providing a basis for developing DEP-based applications for stem cells.

[*]Corresponding Authors: Jente Lu, Department of Biomedical Engineering, University of California at Irvine, 3020 Gross Hall, 845 Health Sciences Road, Irvine, California 92697, Tel: (949) 824-0245, jentel@uci.edu. Lisa A. Flanagan, Ph.D., Department of Neurology, Sue & Bill Gross Stem Cell Research Center, University of California Irvine, 3030 Gross Hall, 845 Health Sciences Road, Irvine, California 92697-1705, Tel: (949) 824-5786, lflanaga@uci.edu.

Keywords

neural stem/progenitor cell; dielectrophoresis; viability; proliferation; cell cycle; fate potential; induced transmembrane potential

INTRODUCTION

Advances in micro-engineered systems for cellular analysis, characterization, and isolation have enhanced understanding of the behavior and function of normal and diseased cells (1). For example, microsystems enabled high throughput single cell molecular analysis (2), precise control of soluble regulators in the cell microenvironment (3, 4), and the formation of organized cellular constructs to create models of organ development or disease (5, 6). Systems incorporating AC electrokinetics, such as dielectrophoresis (DEP), describe the motion of cells induced by non-uniform electric fields without the use of cell type specific labels. DEP has proven useful for patterning a variety of cell types (7–9), isolating cancer cells (10), and enriching platelets and blood cells (11, 12). DEP microsystems are now being applied to the study of stem cells in order to increase the understanding of developmental processes and to improve the use of these cells in therapeutic applications.

DEP microsystems used to profile stem cells have generated information about their distinctive characteristics not accessible with other techniques (13). The potential contributions of DEP to the stem cell field are enormous since identification and isolation of specific cell types is becoming increasingly critical for regenerative medicine. Unique cellular dielectric signatures obtained by DEP distinguish mouse neural stem/progenitor cells (NSPCs) and their progeny, differentiated neurons and astrocytes (14). Furthermore, NSPCs with higher neuron production (neuronal progenitors) have dielectric properties distinct from those of NSPCs with higher astrocyte production (astrocytic progenitors), which is useful since these cells are difficult to distinguish with known biomarkers (14). Recently, cell membrane capacitance measured by DEP has been identified as a biophysical marker indicative of the neurogenic fate potential of both mouse and human NSPCs (15). Similarly, differentiation of adipose-derived stem cells along osteogenic and adipogenic lineages is detected by cell membrane capacitance measured by impedance spectroscopy, which, like DEP, employs a range of frequencies and measures cell biophysical properties (16). Furthermore, membrane capacitance measured by impedance analysis specifically identifies the six main leukocyte subpopulations in the hematopoietic lineage (17). Dielectric properties measured in microsystem platforms can thus serve as label-free indicators of stem cell fate potential and lineage and could be exploited to investigate the biological differences between specific stem and progenitor cells.

Several types of cells, including stem cells, have been successfully separated in DEP microsystems (18). CD34+ hematopoietic stem cells (HSCs) are enriched (5.9-fold increase) from both bone marrow and peripheral blood using DEP (19). Recently, a 14-fold enrichment of NG2+ putative stem cells from adipose tissue was achieved using DEP field-flow fractionation (1.9% to 28%) (20). This study demonstrates that DEP-based stem cell isolation is sufficient to meet the requirements of cell purity for certain clinical applications. DEP enjoys growing prevalence as a label-free isolation method in the stem cell field. Despite this trend, little is known about the potential effects of DEP exposure on stem cell function.

For DEP microsystems to be used successfully for cell manipulation, characterization, and isolation, it is imperative to determine whether exposure to DEP electric fields has any impact on the cells. Attention should be paid to whether the cells are in suspension or

adherent, since the strength of the DEP electric field varies with distance from the electrode. Cells in suspension can move toward or away from electrodes, depending on the frequency and whether they experience positive or negative DEP, so their position relative to the electrode will vary. Adherent cells cannot move away from electrodes in response to negative DEP so are more fixed in position relative to the electric field.

Consequences of DEP exposure have been assessed for a variety of cell types with varying buffer conditions and DEP parameters and have yielded mixed results. DEP exposure does not affect the survival/proliferation of CD34+ cells isolated from peripheral blood (up to 20 sec exposure) (21) nor induce changes in the cell growth curves of suspended K562 leukemia cells (10 min exposure) (22). Exposure to DEP does not alter survival of HL60 leukemia cells in suspension (20 min exposure) (23) and does not affect survival or proliferation of suspended DS19 erythroleukemia cells (30 min exposure) (24). In contrast, when DS19 erythroleukemia cells in media with higher conductivity (300 μS/cm and above) were exposed to particular DEP frequencies, cell survival decreased and cell growth was delayed (30 min exposure) (24). The authors determined these effects were largely due to peroxide formation in the media (24). Additional studies conducted in higher conductivity media document a decrease in the survival of suspended HL-60 leukemia cells (25) and small increases in the stress related gene c-fos in monocytes (26), but no effect on the survival, growth, and secretion of hybridoma or CHO cells in suspension (27). Analysis of the effects of DEP on adherent NIH3T3 fibroblasts demonstrated increasing expression of the stress-related gene Heat Shock Factor 1 with increasing electric field voltage and duration of exposure, which were linked to local heat production (28). Clearly, the impact of DEP microsystems on myriad functions of suspended or adherent cells must be taken into account when interpreting cell biological results obtained in these systems.

Since DEP is proving to be a useful technology for the analysis of stem cells, the influence of electric fields on the stem cell behaviors of self-renewal (proliferation) and differentiation must be carefully considered. Stem cell self-renewal and differentiation are critically important for their use as therapeutics or for the study of developmental biology. Furthermore, analysis of the effects of electric fields should be performed on cells in suspension since they would be in this state for cell sorting and micropatterning applications. In this study, we test whether DEP alters suspended human and mouse NSPC viability, proliferation, or fate potential upon differentiation. We chose DEP parameters to include the range of frequencies used to distinguish distinct NSPCs and differentiated progeny (10 kHz to 1 MHz) (14, 15) and times based on DEP applications: short-term exposure (10 sec to 1 min) for cell sorting and rapid cell patterning (29, 30) and long-term exposure (5 min to 30 min) for extended cell patterning (7). We found no significant impact of DEP on suspended mouse and human NSPC survival, proliferation, and fate potential upon differentiation at any frequency with short-term DEP exposure. However, at frequencies between 50 kHz and 100 kHz there was an approximately 30% decrease in NSPC survival with long-term DEP exposure (10 and 30 min). Although some cells were damaged by long-term DEP exposure at 50 and 100 kHz frequencies, there was no detectable change in proliferation of the surviving cells at those or any other frequencies. Furthermore, the differentiation potential of NSPCs was not altered by any DEP exposure frequency or time. We performed finite element modeling and found that for cells in suspension, cell damage correlates strongly with acute changes in the transmembrane potential at frequencies near the crossover frequency. The maximal impact of frequencies near the crossover frequency would be expected to apply to any cell type in suspension in DEP electric fields. Modeling of electrode size and gap spacing suggest dimensions that allow DEP-induced cell movement but minimize the induced transmembrane potential, which can harm cells. Our results suggest AC electric fields typically used for DEP are not harmful to stem cells if the exposure times are kept low. With the use of appropriate

parameters, DEP microsystems can be utilized for manipulating and sorting NSPCs and may provide unique cellular information not currently available with more widely used methods.

MATERIALS AND METHODS

Ethics statement

All animal housing conditions and dissection procedures were approved by and conducted according to the Institutional Animal Care and Use Committee (IACUC) at the University of California, Irvine. The UC Irvine Institutional Review Board (UCI IRB) approved the use of human stem cells in this study.

Cell culture

Fetal-derived human NSPC cultures (HuNSPC SC27 and SC23) isolated from the brain cerebral cortex at the gestational age of 23 weeks were maintained as previously described (31). All experiments utilized HuNSPCs cultures at passages 8–15. All cell cultures were maintained in a humidified incubator, operating at 37°C with 5% CO_2, until the time of experimentation. Fetal-derived mouse NSPC (mNSPC) cultures were isolated from cerebral cortical regions of wild-type CD1 mice at embryonic day 12.5 (E12.5) and maintained as described (14). Mouse NSPCs were grown as neurospheres in DMEM, B27, N2, 1 mM sodium pyruvate, 2 mM glutamine, 1 mM N-acetylcysteine (Sigma Aldrich, St. Louis, MO), 20 ng/ml epidermal growth factor (BD Biosciences, Bedford, MA), 10 ng/ml FGF (BD Biosciences, Bedford, MA), and 2 μg/ml heparin (Sigma, St. Louis, MO).

Cell preparation for DEP

HuNSPCs were dissociated into a single cell suspension for DEP experiments using non-enzymatic Cell Dissociation Buffer (Invitrogen, Carlsbad, CA). Mouse NSPCs were prepared as a single cell suspension for DEP experiments using non-enzymatic dissociation with NeuroCult (StemCell Technologies, Vancouver, BC, Canada). Dissociated cells were washed once with and resuspended into DEP buffer, an iso-osmotic medium consisting of 8.5% (w/v) sucrose, 0.3% (w/v) glucose, adjusted to a final conductivity of 110 μS/cm using RPMI-1640 medium (14). The conductivity was measured with a conductivity meter (Thermo Orion, Beverly, MA). The final cell concentration was adjusted to 1×10^6 cells/mL for all DEP experiments.

Device Fabrication

DEP multi-well devices (3×5 array) were fabricated on glass slides using methods described previously for the fabrication of a microfluidic channel DEP device (14). Briefly, standard lithography techniques were used to pattern an interdigitated electrode array (200Å titanium and 1000Å gold) on the top of the glass slide with 50 μm-wide electrodes, spaced 100 μm apart. Pre-cured PDMS layers with wells in a 3×5 array were bonded to the glass slides to form the wells. The dimensions of each DEP well are 0.2 cm in diameter and 3 mm in depth. Electric wires were connected to the device electrodes with conductive epoxy (MG Chemicals, Toronto, Ontario, Canada).

DEP exposure

Prior to DEP exposure experiments, the DEP-multi-well device was sterilized by UV light for at least 30 min, followed by washings with 70% EtOH (v/v), mQ H_2O, 0.05% trypsin-EDTA (v/v), and DEP buffer in sequential order in a sterile hood. DEP exposure experiments were performed in the tissue culture hood to maintain sterility of the cells. Dissociated cell suspensions (100 μl) were added to each well followed by a 10 min incubation to allow at least 95% of cells to settle to the bottom of the well, allowing

consistent proximity to electrodes. An AC electric field was applied to the cells using a function generator AFG320 (Tektronix, Beaverton, OR) with 8V $_{\text{peak-peak}}$ for testing frequencies of 10 kHz, 50 kHz, 100 kHz, 400 kHz, 1 MHz, and 10 MHz for DEP exposure times of 10 sec, 1 min, 5 min, 10 min, and 30 min. Post-DEP exposure analysis was performed at the end of each run to evaluate the impact of DEP on cells.

Cell survival assay

The effect of DEP exposure on survival and cell membrane integrity was assessed by calculating the percentage of cells excluding trypan blue using a hemocytometer. Transient membrane disruption was assessed by lactate dehydrogenase (LDH) assay (Clontech, Mountain View, CA). The amount of LDH release was measured using the following equation:

$$\%\text{LDH release} = \frac{(\text{Abs}_{\text{DEP}} - \text{Abs}_{0\%})}{(\text{Abs}_{100\%} - \text{Abs}_{0\%})} \times 100\% \quad \text{(Eq. 1)}$$

where Abs is the absorbance at 490 nm; the subscripts DEP, 0%, and 100%, represent LDH released by DEP-exposed cells, LDH released by maintaining cells in DEP buffer, and complete LDH released by lysing the cells with 0.05% Triton X-100 (Fisher BioReagents, Fair Lawn, NJ) in DEP buffer at 37°C for 10 min, respectively. The absorbance was measured with the KC-4TM microplate reader (Bio-Tek Instruments INC, Winooski, VT) and the levels of released LDH were stable for at least 1 h.

To evaluate the influence of DEP on cellular metabolic activity, the MTT [3-(4,5-dimethylthiazole-2-yl)-2,5-diphenyl tetrazolium bromide] assay kit was used (Invitrogen, Carlsbad, CA). Briefly, cells were incubated in EMEM (without phenol red) supplemented with 0.5% (v/v) L-glutamine and 1 mM MTT, for 4 h post-DEP exposure. MTT was reduced to formazan by cell metabolic activity. To determine the amount of MTT reduction, the formazan was then collected by centrifugation, dissolved in dimethyl sulfoxide (DMSO), measured by a colorimetric method (Abs at 570 nm), and percentage reduction calculated as follows:

$$\%MTT\ reduction = (Abs_{DEP}/Abs_{control}) \times 100\% \quad \text{(Eq. 2)}$$

where Abs_{DEP} and $\text{Abs}_{\text{control}}$ are the absorbances of the DEP exposed sample and the control sample (no DEP exposure), respectively. All post-DEP exposure analyses were performed in at least three independent experiments for each condition.

Cell proliferation assay

The Click-iT EdU kit (Invitrogen, Carlsbad, CA) was used to determine the percentage of HuNSPCs entering S-phase. Immediately following DEP exposure, HuNSPCs were plated on laminin-coated (20μg/ml) coverslips and cultured in HuNSPC growth medium supplemented with 10 μM EdU at 37 °C for 4 h. Cells were fixed, permeabilized, and blocked using 4% PFA, 0.3% Triton X-100, and 5% BSA/PBS solution as described earlier (31). The Click-iT reaction was performed, in which a copper ion (Cu^{+1}) is catalyzed in a covalent reaction with a azide in the Alexa Fluor dye and an alkyne in the EdU molecule for 1 h. Nuclei were counter stained by Hoechst (Invitrogen, Carlsbad, CA). The percentage of cells entering S-phase was determined by quantifying five randomly selected fields for each condition from each experiment.

Cell cycle kinetics was analyzed as described (32). After DEP exposure, HuNSPCs were seeded on fibronectin-coated plates with HuNSPC growth medium. The cells were removed

from plates using cell dissociation buffer at 0, 24, 48, and 96 h post-DEP exposure, fixed using 70% ice-cold ethanol, and stored at −20 °C fridge for at least 24 h. The fixed cells were rehydrated using PBS prior to propidium iodide (PI) staining (2 μg/ml PI with 0.2 mg/ml RNAse in the dark for 60 min) (33). Cell cycle was measured using a Becton-Dickinson LSR-II flow cytometer (BD Biosciences, San Jose, CA) and analyzed using the Dean-Jett-Fox model in FlowJo (Treestar, Ashland, OR) with the constraint on the position of G2 peak to be 2 times the G1 peak to provide the best-fit results for HuNSPCs.

Cell differentiation/Fate potential Assay

The percentage of HuNSPCs fated to the neuronal lineage was determined by differentiation of cells for 2 weeks in differentiation media (15, 31). Neurons were Map2-positive cells with neurites at least 3× the length of the cell body, which has been shown to reflect the percentage of cells co-stained by Map2 and doublecortin, an early neuronal marker, for HuNSPCs (15). For astrocyte differentiation, cells were differentiated in DMEM-F12 with 20% FBS for 1 week. Astrocytes were GFAP-positive and Sox2-negative cells, which distinguished them from GFAP-expressing NSPCs (15, 34). At least 500 cells were counted for each experimental condition from images of five randomly selected fields. The double-blind method was used to quantify all fields for each condition.

Immunostaining

Immunostaining was as previously described (31), and the following antibodies were used: anti-Sox2 (Y-17) polyclonal, 1:100 (Santa Cruz Biotechnology, Santa Cruz, CA); anti-Nestin polyclonal, 1:100 (Chemicon, Temecula, CA); anti-GFAP (clone G5A) monoclonal, 1:200 (Sigma, St. Louis, MO); anti-MAP2 (microtubule-associated protein 2) (HM2) monoclonal, 1:100 (Sigma, St. Louis, MO). The secondary antibodies were donkey anti-mouse Alexa Fluor 555 and donkey anti-goat/rabbit Alexa Fluor 488, dilution of 1:100 (Molecular Probes/Invitrogen, Carlsbad, CA).

Electric field simulation and estimation of induced transmembrane potential

Computational fluid dynamics (CFD) software (CFD-ACE+; ESI, Huntsville, AL) was used to determine the electric field distribution in each DEP well. To accurately estimate the electric field at each cell location, the gravitational and dielectrophoretic forces were both considered (details in Supporting Material).

After deriving the equilibrium position of the cells and determining the electric field, the induced transmembrane potential, ΔU, was calculated as described (35). In brief, the cells are assumed in this model to be homogenous spheres with an insulating bilipid membrane, which is described as:

$$\Delta U = \frac{(3/2) \times E \times r \times \cos\theta}{1 + r \times (G_{mem} + j\omega C_{mem})(\rho_i + \rho_s/2)} \quad \text{(Eq. 3)}$$

where ΔU is a function of the applied electric field E and the angular frequency ω ($\omega = 2\pi f$). C_{mem} and G_{mem} are the specific membrane capacitance and conductance, respectively. ρi and ρs are the resistance of the cell interior and suspending medium, respectively, and were assumed as 90.9 ohm and 1 ohm (35). The radius of the cell is r. The polar angle with respect to the electric field is represented by θ. Values are listed in Table S1 in Supporting Material. The induced transmembrane potential was numerically solved by commercial software MATLAB (Version 7 R13, The MathWorks, Natick, MA).

Electrode configuration optimization

To determine the optimized electrode configuration for maximum cell movement and minimum effects on the cell membrane we performed two simulations. In the first, a parametric optimization model for movement was established by simulating the trajectory of a particle in a microchannel with multiple electrode configurations in the lower side of the wall using CFD-ACE+ (ESI, Huntsville, AL). In brief, a microfluidic channel with a steady-state laminar fluid flow in the x-direction and no flow in the y-direction at all locations is set as the initial condition. The total bulk flow rate in the microchannel was set to 1 mL per minute at the inlet and the pressure at the outlet was set to the reference pressure of 100 kPa. A no-slip boundary condition was applied to all the walls within the microchannel. A 14 μm polystyrene bead (approximately the size of a single NSPC) was placed at the bottom of the channel (7μm above the surface) near the inlet (Fig. 7A).

An applied voltage of 8V $_{\text{peak-peak}}$ was used. The inlet, outlet, gaps between electrodes, and the rest of the walls were set as insulator. The applied frequency was set at the value that the maximal negative DEP force would be induced on the particle with Re = −0.5 (the parameters used in simulating the particle deflection are listed in Table S2 in Supporting Material). Particle trajectories, delta Y (Δy), were obtained by calculating the displacement of the particles between initial y, y_{initial}, and terminal y value, y_{final}, with and without the DEP force:

$$\nabla y = y_{\text{final}} - y_{\text{initial}} - \nabla y_{\text{no-DEP}} \quad \text{(Eq. 4)}$$

where $\Delta y_{\text{no–DEP}}$ represent the particle deflection due to flow without DEP force. The deviation was defined as the lateral displacement of a particular particle entering the channel along the lower wall. This corresponds to the maximum displacement that the electrode configuration can impart on a particle at a given constant flow speed. Electrode and gap widths were varied from 25–500 μm and the modeling run to calculate predicted deflecting distances.

The second simulation was run to determine electrode configurations with minimum effects on the cell membrane. Using CFD-ACE+ as described above, we increased the numbers of electrodes, used similar initial and boundary conditions, but removed the polystyrene bead in the model. We then derived the average electric field on the surface of electrodes for multiple electrode/gap configurations. Since the electric field is proportional to induced transmembrane potential (Eq. 3), these values give an estimate of the potential for cell disruption with each electrode and gap configuration. Electrode and gap widths were varied from 25–500 μm and the voltage was 8V $_{\text{peak-peak}}$ (the parameters used are listed in Table S2 in Supporting Material).

Statistical analysis

Statistical analyses used Student's t test, and p-value < 0.05 was considered significant. All data are expressed as means ± SE of at least three independent experiments.

RESULTS

Devices and parameters for testing effects of DEP on NSPCs

The experimental setup used to evaluate the impact of DEP on stem cells is illustrated in Fig. 1A. The DEP device was fabricated as a multiplex well platform with interdigitated electrodes on the bottom of each well. Each array is connected to a single circuit and consists of three wells for triplicates within each experiment (blue box, Fig. 1A). DEP force exposure for each condition is controlled by a function generator connected to switches for

each circuit. The design of the interdigitated electrodes at the bottom of each well mimics that used for characterization of mNSPC's dielectric properties (14).

We assessed the impact of DEP on HuNSPCs (SC27 and SC23, Fig. 1B) since human cells are relevant for therapeutic purposes and mouse NSPCs (embryonic day 12.5, E12.5) to determine whether the results apply to multiple species and types of NSPCs. Prior to analysis, NSPCs were suspended in DEP buffer and loaded into each well of a DEP multiplex platform for DEP exposure (Fig. 1). Using cells in suspension not only matches the cell status needed for rapid DEP sorting or patterning of NSPCs, but also satisfies the assumptions made for the single shell model (See Supporting Materials) and thus reduces errors in estimating the induced DEP force. We tested whether DEP exposure affects NSPC survival, proliferation, and differentiation.

Effect of short-term DEP exposure on NSPC survival

We implemented three discrete assays to fully investigate the physiological impact of DEP on NSPC survival: trypan blue exclusion as a measure of cell death, LDH release to track membrane permeabilization, and MTT reduction to assess mitochondrial function and metabolism. The design of experiments to evaluate cell viability for short-term DEP exposure, such as needed for cell sorting, and long-term DEP exposure as envisioned for extended cell patterning is shown schematically in Fig. 2A.

No significant cell death of HuNSPCs (SC27) was detected by trypan blue staining with short-term DEP exposure (up to 1 min) at all applied frequencies (Fig. 2B). We expanded the study to a second set of HuNSPCs (SC23) and to mNSPCs (E12.5) and found similar results (Figs. 2C, S2A, and S3A). NSPCs under normal growth conditions do not release much LDH (Fig. S1), so we used LDH release as a measure of cell membrane integrity and found no significant difference between controls and cells exposed to 10 kHz, 100 kHz, and 1 MHz DEP frequencies (Fig. 2D). However, a small but statistically significant amount of transient membrane disruption occurred at 50 kHz (Fig. 2D, cells exposed to 50 kHz for 60 sec LDH release 12.8%, $p < 0.01$). The same trend held true for HuNSPCs (SC23) and mNSPCs (E12.5) with more LDH release from cells exposed to 50 kHz DEP (Figs. S2C and S3C; SC23: cells exposed to 50 kHz for 60 sec LDH release 10.6%, $p<0.01$; E12.5: cells exposed to 50 kHz for 60 sec LDH release 9.8%, $p < 0.01$). For all NSPCs tested, the transient membrane permeability induced by 50 kHz DEP exposure did not result in cell death as measured by trypan blue exclusion (Figs. 2B, S2A, and S3A). In order to clarify whether DEP exposure and the small transient membrane permeability induced by 50 kHz DEP alter cellular function, we employed the MTT assay to measure NSPC's mitochondrial activity and metabolism. Although the cell viability and membrane permeability data were fairly consistent across the three sets of NSPCs, there was greater variability in mitochondrial function of the cells after 60 sec DEP exposure. There was no significant decrease in the metabolic activity of SC27 HuNSPCs exposed to 50 kHz, 100 kHz, or 1 MHz DEP, but a very mild decrease in cells exposed to 10 kHz (Fig. 2E, 9.3% decrease in 10 kHz exposed cells; $p < 0.05$). In contrast, the mitochondrial function of SC23 HuNSPCs was not affected by 10 kHz, 100 kHz, or 1 MHz DEP exposure but was somewhat decreased by 50 kHz exposure (Fig. S2E, 20.5% decrease in 50 kHz-exposed cells; $p < 0.05$). Mouse E12.5 mNSPCs were similarly not altered by 10 kHz or 1 MHz DEP exposure, but did exhibit mild decreases in mitochondrial activity after exposure to 50 kHz and 100 kHz DEP (Fig. S3E, 14.6% decrease in 50 kHz exposed cells and 10.6% decrease in 100 kHz-exposed cells, $p < 0.05$). Notably, the changes in mitochondrial function as revealed by the MTT assay were small in all cases and did not correlate well with cell death or transient membrane permeability after short-term DEP exposure as shown by the other assays. The lack of consistent effects on mitochondrial function among the three sets of NSPCs suggests cell-specific changes in metabolic activity in response to DEP exposure might exist. Most

importantly, the survival and function of NSPCs evaluated by all three different assays remained greater than 87% after exposure to all DEP frequencies. These results suggest that short-term DEP exposure has negligible, if any, adverse effects on NSPC survival.

Effect of long-term DEP exposure on NSPC survival

We extended the DEP exposure time to 30 min to elucidate whether DEP is also non-toxic for cell patterning applications demanding long-term DEP exposure (7). A small decrease in HuNSPC (SC27) viability occurred at 5 min only at 50 kHz frequency (12.8% decrease, $p < 0.05$) and at 10 min at 50 kHz and 100 kHz frequencies (16.3% decrease in 50 kHz-exposed cells and 21.2% decrease in 100 kHz-exposed cells, $p < 0.01$) (Fig. 3A). After 30 min DEP exposure, up to 29.8% and 27.2% of the cells incurred damage at 50 kHz and 100 kHz, respectively, but no significant damage occurred at 10 kHz, 400 kHz, 1 MHz, and 10 MHz. Moreover, survival of SC23 HuNSPCs and E12.5 mNSPCs was also not altered by up to 30 min exposure to 10 kHz, 400 kHz, 1 MHz, and 10 MHz frequencies but was compromised by 30 min exposure to 50 kHz or 100 kHz frequencies (Fig. 3B, S2B and S3B). Neither SC23 HuNSPCs nor E12.5 mNSPCs were significantly affected by 5 min DEP exposure at any frequency, but 10 min DEP exposure damaged SC23 cells at 50 kHz and E12.5 cells at 100 kHz (Figs. S2B and S3B, $p <0.05$). Interestingly, the frequency at which cells experience maximal damage differs for human and mouse NSPCs; the frequency causing the greatest loss of cell viability is 50 kHz for HuNSPCs (SC27 and SC23) and 100 kHz for mNSPCs (Figs. 3B, S2B, and S3B). For all three sets of NSPCs, long-term (30 min) exposure to 10 kHz, 400 kHz, 1 MHz, and 10 MHz frequencies did not alter cell survival but 50 kHz and 100 kHz frequencies decreased cell survival by up to 30%.

We evaluated cell membrane integrity after long-term DEP exposure by measuring release of LDH from the cells. Exposure of human or mouse NSPCs to 1 MHz DEP for up to 30 min either did not alter or only induced minor increases (10% or less) in LDH release (Figs. 3C, S2D, and S3D). Long-term exposure to 10 kHz caused minor LDH release from SC27 HuNSPCs and E12.5 mNSPCs, but a slightly greater amount of LDH release from SC23 HuNSPCs (Figs. 3C, S2D, and S3D). The maximum release of LDH from HuNSPCs (SC27 and SC23) occurred after 30 min exposure to 50 kHz (Figs. 3C and S2D). E12.5 mNSPCs released roughly equivalent amounts of LDH after 30 min exposure to 50 kHz and 100 kHz frequencies (Fig. S3D). The amount of LDH released by HuNSPCs (SC27 and SC23) after 30 min exposure to 100 kHz matches relatively well with the percentage of dead or dying cells detected by trypan blue exclusion (Figs. 3 and S2). In contrast, HuNSPCs exposed to 50 kHz DEP for 30 min released a greater amount of LDH than the percentage of damaged cells determined by trypan blue exclusion (Figs. 3 and S2; SC27 ~50% LDH release and ~25% dead or dying by trypan blue; SC23 ~45% LDH release and ~35% dead or dying by trypan blue). These data imply that while some cells experience transient membrane permeability during 50 kHz DEP exposure, they are able to restore membrane integrity and do not die. Evidence for transient membrane permeability of HuNSPCs during exposure to 50 kHz DEP frequency was obtained in both short-term and long-term DEP experiments (Figs. 2 and 3).

We measured NSPC mitochondrial activity and metabolism with the MTT assay after long-term DEP exposure. All NSPCs exposed to 10 kHz or 1 MHz frequencies for 10 or 30 min showed no change or minor (<10%) decreases in metabolic activity (Figs. 3D, S2F, and S3F) SC27 HuNSPCs exposed to 50 kHz and 100 kHz frequencies showed an approximately 25% decrease in metabolic activity (Fig. 3D). The effect of these two frequencies on the cells was similar, which was also the case for cell survival as measured by trypan blue staining (Fig. 3A), and the percent decrease in metabolic activity matches well with the percentage of dead or dying cells detected by trypan blue (Figs. 3A and 3D). In contrast, SC23 HuNSPCs exposed to long term DEP at 50 kHz had a much greater decrease

in metabolic activity than those subjected to 100 kHz (Fig. S2F). As seen with LDH release from these cells, the extent of metabolic disruption induced by 50 kHz frequency was greater than the amount of cell death at 30 min detected by trypan blue staining (Figs. S2B, S2D, and S2F). Mouse NSPCs respond similarly to 50 kHz and 100 kHz frequencies in all assays (trypan blue, LDH, and MTT) and the change in metabolic activity of cells exposed to these frequencies was similar to the change in LDH release and higher than the amount of cell death determined by trypan blue staining (Figs. S3B, S3D, and S3F). Based on these results, the responses of different sets of NSPCs to particular DEP frequencies may vary. Taken together, the results from the cell survival assays demonstrate that frequencies in both the negative (10 kHz) and positive (400 kHz, 1 MHz, 10 MHz) DEP ranges do not appreciably alter NSPC survival even after 30 min exposure. However, prolonged exposure of NSPCs to DEP frequencies near the crossover frequency in the 50–100 kHz range decreased cell survival by ~30%.

Influence of short and long term DEP exposure on NSPC proliferation

Testing the effects of DEP on NSPC proliferation is imperative since DEP exposure may alter cell cycle kinetics (24) and our analysis of cell survival demonstrated that a percentage of NSPCs experience transient membrane permeability after exposure to certain DEP frequencies (Figs. 3, S2, and S3). We used EdU incorporation and cell cycle kinetics assays to test the proliferative ability of NSPCs exposed to DEP for 1 min and 30 min in order to compare results with those obtained for cell survival after short and long term DEP exposure as described above (experimental design depicted in Fig. 4A). Short-term (1 min) DEP exposure did not alter the percentage of cells in S phase shortly after DEP (Fig. 4B) or the cell cycle kinetics of NSPCs up to 4 days after DEP (Fig. S4). There was also no significant effect of long term (30 min) DEP exposure on the percentage of cells in S phase, although there was higher variability among HuNSPCs exposed to 10 kHz for 30 min (Fig. 4B). Long-term DEP exposure did not affect NSPC cell cycle kinetics since there was no difference in the percentages of cells in each stage of the cell cycle between controls and exposed cells (Fig. 4C). Similar results with SC23 HuNSPCs and E12 mNSPCs were obtained in the EdU and cell cycle kinetics assays (data not shown). Evaluation of cell division with two independent methods spanning a range of times after DEP clarifies that DEP exposure does not have a significant impact on the proliferation of NSPCs.

Impact of DEP exposure on NSPC differentiation potential

An important characteristic of stem cells is their ability to differentiate into mature cells to form organs and tissues. We tested whether exposure to DEP frequencies altered the differentiation of SC27 HuNSPCs by exposing the cells to various frequencies for 30 min and inducing differentiation afterward by changing the cell substrate and media composition (Fig. 5A) (31). CNS NSPCs generate three cell types: neurons, astrocytes, and oligodendrocytes. We measured generation of neurons and astrocytes, but not oligodendrocytes since special hypoxic conditions are required to generate these cells from HuNSPCs in vitro (36). No significant difference was found in the percentages of neurons or astrocytes differentiated from control HuNSPCs and those exposed to DEP (Figs. 5B–E). Therefore, the lineage potential, namely whether cells differentiate into neuronal or astrocytic lineages, of HuNSPCs was not altered by 30 min exposure to DEP frequencies ranging from 10 kHz to 1 MHz.

DEP-induced NSPC membrane disruption correlates with increased induced transmembrane potential

We sought to uncover the mechanism by which long-term DEP exposure to frequencies ~50–100 kHz induced transient membrane disruption or cell death for some NSPCs. Finite element modeling and numerical simulations were utilized to clarify the strength of the AC

electric field within the DEP device. According to the modeling, the gradient of the electric field square varies with the distance from the electrodes, with the strongest electric field being adjacent to the electrode edges (Fig. 6A). Therefore, the closer cells are to the electrodes, the stronger the electric field they will experience.

The cells in our analysis are in suspension and their movement in the electric field is governed by the Clausius-Mossotti (CM) factor. The CM factor is frequency-dependent and takes into account the dielectric properties of the cell, such as the membrane permittivity, which is related to capacitance, and membrane conductivity (see S Eqs. 2–5 in Supporting Material). The CM factor is proportional to the induced DEP force for that cell (Fig. 6B, S Eq. 1 in Supporting Material). The CM factor in combination with the gravitational force (S Eqs. 6–7 in Supporting Material) determines the position of cells in suspension relative to the electrodes. Thus, applied frequencies below the crossover frequency of SC27 HuNSPCs (~45 kHz, red dotted line in Fig. 6B) will induce a negative DEP (nDEP) force that repels cells away from the edge of electrodes while frequencies above the crossover frequency result in positive DEP (pDEP), an attractive force. Strong nDEP forces, such as experienced by HuNSPCs at 10 kHz, repel cells from electrodes and increase the distance between the cells and the electrodes (Fig. 6C, HuNSPCs repelled ~90 mm above electrodes at 10 kHz, see S Eq. 7 in Supporting Material). Strong pDEP forces, experienced by HuNSPCs at 1 MHz, attract cells to electrodes and greatly decrease the distance between cells and electrodes, whereas weak pDEP forces near the crossover frequency (such as 50 kHz) provide a muted attraction toward electrodes (Fig. 6C). The position of the cells relative to the electrodes at each frequency is based on movement of the cells in response to the induced DEP force and the gravitational force.

Time lapse imaging of the movement of cells at frequencies near the crossover frequency shows that cells move within a ~50 μm zone near the electrode (Fig. 6D). In general, three distinct cell behaviors were observed near the crossover frequency: attraction to electrodes with bouncing behavior due to cycles of attraction and repulsion with some cells bursting at the end, attraction to electrodes without continued movement in the zone near the electrode, and attraction followed immediately by cell bursting. Cell bursting is likely due to an irreparable loss of membrane integrity followed by cell swelling and death. For cells in suspension, a given cell's position relative to the electrode at each frequency will vary over a relatively short time course (sec). This means cells rapidly move in and out of regions of high electric fields.

It was reported earlier that exposure to nDEP causes cell membrane disruption due to a significant increase in the transmembrane potential [see Eq. 3] (37, 38). We used a numerical simulation to predict the induced transmembrane potential of NSPCs that do not move in response to the DEP electric field (i.e. adherent cells), and found the induced transmembrane potential is highest at lower frequencies (< 10 kHz), confirming previous results (37, 38) (Fig. 6E, parameters in Table S1 in Supporting Material). In previous studies as well as in our analysis, at voltages less than or equal to $8V_{peak\text{-}peak}$ the higher frequencies such as 1 MHz that cause pDEP do not induce a transmembrane potential even though the cells are very close to the electrodes and thus in a strong electric field (Fig. 6E).

We found a very different pattern of induced transmembrane potential for cells that are in suspension, and thus able to move in the electric field (see S Eq. 7 in Supporting Materials for calculation of the position of the cells relative to the electrodes). Simulation of cells in suspension showed that the induced transmembrane potential is highest near the crossover frequency (in this case ~50 kHz) and lower at frequencies below and above this region (Fig. 6F). Therefore, nDEP (e.g. 10 kHz for HuNSPCs) does not induce a large transmembrane potential for cells in suspension since they are repelled to a weaker region of the electric

field. Near the crossover frequency, the cells are maintained in a stronger region of the electric field and those frequencies therefore do induce a transmembrane potential. The position of the cells relative to the electrodes affects the induced transmembrane potential, so cells that bounce near the electrode experience radical and rapid shifts in induced transmembrane potential (Fig. 6D and 6F). As seen for the adherent cell simulation, strong pDEP frequencies do not induce a transmembrane potential for cells in suspension (Fig. 6E–F). Our experimental data and simulations demonstrate that for cells in suspension, frequencies near the crossover frequency are more likely to be toxic by perturbing the cell membrane than lower, nDEP, or higher, pDEP, frequencies. This is in contrast to the situation for adherent cells, where lower, nDEP frequencies would be the most damaging.

Modified electrode configurations reduce electric field exposure

Our analysis of the effects of DEP electric fields on NSPCs caused us to wonder whether the interdigitated electrode design we used was optimal for allowing the lowest possible exposure to the electric fields. Ideally, DEP devices would contain configurations of electrodes and the gaps between them that maximize the induced DEP force (for cell movement) while minimizing the induced transmembrane potential that disrupts cell membrane integrity. We did modeling to predict electrode and gap configurations that would produce maximal cell movement and compared those to modeling of the electric field to estimate the generation of an induced transmembrane potential. Parametric CFD modeling was used to determine the maximal movement, or deflection, of cell-sized particles away from electrodes with various electrode and gap sizes (electrode and gap widths ranging from 25–500 μm, see Materials and Methods for modeling details). Particle defection was modeled in the presence of fluid flow since many DEP devices would incorporate fluid to load cells into the device or move cells across the DEP electrodes. The modeling showed that electrode widths of 200–400 μm and gap widths of 25–40 μm give maximal deflection (Fig. 7A). Our current design of 50 μm electrodes and 100 μm gaps provides an intermediate level of deflection.

To compare electrode configurations for cell disruption, we modeled the electric field for each size electrode and gap since the electric field strength is proportional to the induced transmembrane potential (Eq. 3) and probability of cell damage. We calculated the mean electric field per electrode pair near the edge of each electrode (Fig. 7B, left panel) since this region of the electric field was associated with greater cell disruption (Fig 6). As shown in Figure 7B right panel, an inverse correlation was found between gap size and the mean electric field. As the gap increases in size, the mean electric field decreases substantially. Gap size also interacts with electrode size, as has been shown for nDEP devices (39). For gap sizes of 200 μm and greater, changing electrode width from 25–500 μm makes little difference to the mean electric field. On the other hand, for gap sizes of 25–100 μm decreasing electrode width leads to increasing mean electric field, reaching a maximum at 50 μm electrode width. The mean electric field drops dramatically with 25 μm electrode width. The electrode and gap configuration of our DEP device (50 μm electrode × 100 μm gap) would give an intermediate mean electric field and induced transmembrane potential, which could be lessened by increasing the gap size. We calculated the expected average induced transmembrane potential for SC27 HuNSPCs at 50 kHz for the 400 μm electrode and 25 μm gap configuration and found that the value was reduced by ~30% from that of our 50 μm electrode and 100 μm gap configuration. Combining the simulated deflecting distance and the mean electric field of various electrode and gap configurations suggests that a 400 μm electrode width with 25–50 μm gaps would provide a reasonable balance of cell movement and viability in DEP devices.

DISCUSSION

Utilizing DEP for stem cell sorting or manipulation requires examining whether DEP exposure is associated with any adverse effects on cell physiology since truly enabling biotechnologies must pay careful attention to their biological effects as well as their technological advances. This study contains three main conclusions regarding the cellular consequences of AC electric field exposure in DEP microsystems. Firstly, exposure to AC electric fields causes changes in membrane permeability that can be transient or permanent depending on the applied DEP frequency and exposure time. Our detailed analyses show that NSPCs able to repair leaky membranes do not sustain damage that alters mitochondrial function and metabolism, cell proliferation and cell cycle kinetics, or differentiation of the cells into neurons or astrocytes. Secondly, cells in solution (as would be common for many DEP applications) experience effects on the cell membrane at frequencies near the crossover frequency rather than negative DEP frequencies as previously reported for adherent cells. We show that for cells in suspension the key is the interaction of the induced transmembrane potential, the strength of the electric field at specific distances from the electrodes, and the cell position within the electric field, which is determined by DEP forces that cause cell movement. Lastly, DEP device parameters can be modified to reduce the cell's electric field exposure. Careful consideration of the electrode configuration, length of exposure time, and electric field voltage can mitigate the deleterious effects observed for a subset of NSPCs. These primary findings regarding the specific effects of DEP microsystem electric fields on NSPCs define parameters under which these devices can be safely used for stem cell analysis and sorting.

The time of exposure to electric fields and the DEP frequency determine whether cell membrane permeability is induced and whether the change to the membrane is permanent, resulting in cell death. Combining three separate assays (trypan blue, LDH, and MTT) to evaluate the influence of DEP exposure on cell survival allowed us to determine relationships between membrane integrity, metabolic function, and cell death. For instance, minor and transient membrane disruption was found with short-term DEP exposure (LDH release, Fig. 2 D) that did not lead to cell death or mitochondrial dysfunction (Fig. 2 B, C, E). When the exposure time was increased at certain frequencies, an irreversible membrane disruption occurred that led to mitochondrial dysfunction and cell death in a subset of cells (Fig. 3). Losses in mitochondrial function of SC27 HuNSPCs mirror death of the cells (MTT and trypan blue, Fig. 3), fitting a model in which induced transmembrane potential of the plasma membrane occurs first and leads to membrane disruption that affects mitochondrial function. In our experiments, NSPCs exposed to 30 min DEP at 50 kHz had a greater degree of LDH release than cell death (50% LDH release while 25% cell death by trypan blue or MTT assays, Fig. 3), suggesting ~25% of the cells experienced permanent membrane disruption and cell death, ~25% transient membrane permeability, while ~50% of the cells had no change in membrane integrity. Gascoyne and Vykoukal describe the idea of transient and permanent DEP-induced membrane disruption as "electropermeabilization", in which lower strength electric fields can be utilized to introduce reagents into cells and higher strength fields to lyse cells (40). The data from our cell survival assays demonstrate that NSPCs exposed to DEP undergo dynamic changes of the plasma membrane that are in many cases reversible but at certain frequencies and long exposure times cause death for a subset of the cells.

NSPCs exposed to DEP electric fields exhibited normal proliferation and differentiation along neuronal and astrocytic lineages (Figs. 4, 5). Neither the percentage of NSPCs in S phase nor the cell cycle kinetics of NSPCs over two cell doublings is altered by DEP exposure of any duration or frequency. In contrast, DS19 erythroleukemia cells in suspension arrest at the G2/M phase of the cell cycle after negative DEP exposure when in a

higher conductivity (300–560 μS/cm) DEP buffer but not when a lower conductivity (100 μS/cm) buffer was used, likely due to generation of reactive oxygen species in the higher conductivity buffer (24). We found NSPC differentiation into neurons and astrocytes was normal after all DEP exposure times and frequencies, although other studies have shown links between cell membrane potential or electrical stimulation and differentiation. Inward rectifier potassium channels regulate membrane potential and differentiation of myoblasts (41) and hematopoietic progenitor cells (42) and electrical stimulation of mouse ES cells in an electroporator cuvette increased the generation of neurons from these cells (43). Although there are reports in the literature suggesting that DEP electric field may affect cell proliferation or differentiation, we find no effect of DEP exposure at any duration or frequency on the proliferation or differentiation of NSPCs.

The consequences of DEP exposure differ for cells in suspension and adherent cells. Clarifying the impact of DEP on suspended stem cells is logical since cells would be in solution for many DEP applications such as sorting and micropatterning. Our results show the main effect of DEP on the plasma membranes of suspended NSPCs occurs at applied DEP frequencies near the cell's crossover frequency. Maximal cell damage after 30 minutes DEP exposure occurred at 50 kHz for SC23 and SC27 HuNSPCs, which have crossover frequencies of ~38 kHz and ~45 kHz respectively, and at 100 kHz for E12 mNSPCs, whose crossover frequency is at ~63 kHz (15) (Figs. 3B, S2B, and S3B). Calculating the effects of DEP on cells in suspension is complicated since the cells move in response to the electric field. Our modeling incorporates this cell movement by using NSPC membrane biophysical parameters of capacitance and conductance (15) to calculate the induced DEP force for those cells. The combination of this force and the gravitational force dictate the cell's position in the electric field and the strength of the electric field at that position contributes to the induced transmembrane potential. At higher levels, the induced transmembrane potential may damage the cell's plasma membrane. We show that the induced transmembrane potential for cells in suspension is greatest near the crossover frequency since the cells are drawn to the high strength region of the electric field (Fig 6).

The effects of DEP on other types of cells in suspension have also been linked to the crossover frequency. For example, the induced transmembrane potential of suspended DS19 leukemia cells was highest near the crossover frequency (24), and suspended Jurkat T cells and HL60 leukemia cells were most damaged by frequencies immediately above their crossover frequencies (25). In contrast, adherent rat neuronal cells were damaged by lower frequencies that would correspond to negative DEP rather than frequencies near the crossover frequency (37). Similarly, adherent NIH3T3 fibroblasts expressed greater levels of stress-related genes at low frequencies that would be in the negative DEP range (28). As our modeling in Fig. 6E and 6F shows, the induced transmembrane potential caused by DEP exposure will greatly differ for adherent cells and cells in suspension at frequencies in the negative DEP range since cells in suspension are able to escape the high region of the electric field.

Lastly, several DEP parameters can be modified to further reduce the toxicity experienced by a subset of cells at specific frequencies. Limiting the DEP exposure time of NSPCs to short time scales as would be used for DEP-based cell sorting and rapid cell patterning (30) eliminate all deleterious effects of DEP (Fig. 2). Optimizing the design of DEP electrode arrays by controlling the size of the electrodes and gaps between them can reduce the electric field exposure that may damage the membranes of a subset of cells at longer exposure times (Fig. 7). A wide variety of electrode designs have been developed for DEP and have been recently reviewed (44). Decreasing the applied voltage also reduces electric field strength and may minimize membrane disruption at longer exposure times. For example, reducing voltage from $8V_{peak\text{-}peak}$ to $3V_{peak\text{-}peak}$ with a single electrode design of

50 μm electrodes and 100 μm gaps greatly decreased the percentage of dead or dying NSPCs detected by trypan blue (data not shown). Similarly, higher voltages were associated with greater expression of stress-related genes in adherent fibroblasts (28) and decreased survival of neurons (37). Finally, frequencies near the crossover frequency only perturb a subset of NSPCs and the percentage of affected cells does not greatly increase with longer exposure times (data not shown). We suspect these frequencies target a phenotypically distinct subset of stem or progenitor cells and could potentially be used to selectively ablate specific cell populations within a heterogeneous mix of cells. Supporting this idea, the percentage of SC27 HuNSPCs damaged by long-term DEP exposure at 50 kHz is ~25%, which is similar to the percentage of cells in that population whose crossover frequency is near 50 kHz (~25%, data not shown). Further investigation will be necessary to determine whether selective destruction of a subset of cells would be a useful way to remove undesired cell types in stem cell populations. Correctly choosing DEP parameters can greatly reduce the risk of cell damage by DEP electric fields.

CONCLUSION

The conclusions drawn from our studies of the effects of DEP on cells cross traditional disciplinary boundaries and will have broad significance to the fields of cell electrophysiology and biophysics, microtechnology, AC electrokinetics, and stem cell biology. As microtechnologies such as DEP become increasingly utilized in cell biological applications it will be critical to explore effects of the technology on cell-type specific behaviors. Our description of the effects of DEP on NSPCs would be expected to apply to any cell type in suspension in DEP electric fields, particularly since suspended cells would likely sustain maximal impact near the crossover frequency from the high regions of the electric field. The transient membrane disruption that does not compromise cell viability at certain frequencies and times of DEP exposure may prove useful for the introduction of biological mediators into cells without harming cell function. Careful studies of the effects of DEP on cell function define parameters under which these devices can be safely used for cell analysis and sorting by taking into account the time of exposure, DEP frequency and voltage, and the DEP microsystem electrode design.

Supplementary Material

Refer to Web version on PubMed Central for supplementary material.

Acknowledgments

The authors thank Dr. Philip H. Schwartz for the human NSPCs, Dr. Diane K. O'Dowd for providing the resting membrane potential for SC27 HuNSPCs, Dr. Edwin S. Monuki for critical reading of the manuscript, and Vanessa Scarfone and Christina Tu for technical assistance with flow cytometry. This work was supported in part by the California Institute for Regenerative Medicine (CIRM) RT1-01074, NIH AG23583, and UL1 RR031985 from the National Center for Research Resources (NCRR), a component of the National Institutes of Health (NIH) and the NIH Roadmap for Medical Research. Jente Lu is a pre-doctoral fellow on the UCI CIRM training grant (TG2-01152).

References

1. Toh YC, Blagovic K, Voldman J. Advancing stem cell research with microtechnologies: opportunities and challenges. Integrative biology : quantitative biosciences from nano to macro. 2010; 2(7–8):305–25. Epub 2010/07/02. [PubMed: 20593104]
2. Narsinh KH, Sun N, Sanchez-Freire V, Lee AS, Almeida P, Hu S, et al. Single cell transcriptional profiling reveals heterogeneity of human induced pluripotent stem cells. The Journal of clinical investigation. 2011; 121(3):1217–21. Epub 2011/02/15. [PubMed: 21317531]

3. Blagovic K, Kim LY, Voldman J. Microfluidic perfusion for regulating diffusible signaling in stem cells. PloS one. 2011; 6(8):e22892. Epub 2011/08/11. [PubMed: 21829665]
4. Chung BG, Flanagan LA, Rhee SW, Schwartz PH, Lee AP, Monuki ES, et al. Human neural stem cell growth and differentiation in a gradient-generating microfluidic device. Lab on a chip. 2005; 5(4):401–6. [PubMed: 15791337]
5. Elliott NT, Yuan F. A review of three-dimensional in vitro tissue models for drug discovery and transport studies. Journal of pharmaceutical sciences. 2011; 100(1):59–74. Epub 2010/06/10. [PubMed: 20533556]
6. Huh D, Matthews BD, Mammoto A, Montoya-Zavala M, Hsin HY, Ingber DE. Reconstituting organ-level lung functions on a chip. Science (New York, NY). 2010; 328(5986):1662–8. Epub 2010/06/26.
7. Albrecht DR, Underhill GH, Wassermann TB, Sah RL, Bhatia SN. Probing the role of multicellular organization in three-dimensional microenvironments. Nature methods. 2006; 3(5):369–75. [PubMed: 16628207]
8. Ho CT, Lin RZ, Chang WY, Chang HY, Liu CH. Rapid heterogeneous liver-cell on-chip patterning via the enhanced field-induced dielectrophoresis trap. Lab on a chip. 2006; 6(6):724–34. [PubMed: 16738722]
9. Tsutsui H, Yu E, Marquina S, Valamehr B, Wong I, Wu H, et al. Efficient dielectrophoretic patterning of embryonic stem cells in energy landscapes defined by hydrogel geometries. Annals of biomedical engineering. 2010; 38(12):3777–88. Epub 2010/07/09. [PubMed: 20614250]
10. Huang Y, Yang J, Wang XB, Becker FF, Gascoyne PR. The removal of human breast cancer cells from hematopoietic CD34+ stem cells by dielectrophoretic field-flow-fractionation. J Hematother Stem Cell Res. 1999; 8(5):481–90. [PubMed: 10791899]
11. Han KH, Frazier AB. Lateral-driven continuous dielectrophoretic microseparators for blood cells suspended in a highly conductive medium. Lab on a chip. 2008; 8(7):1079–86. Epub 2008/06/28. [PubMed: 18584082]
12. Pommer MS, Zhang Y, Keerthi N, Chen D, Thomson JA, Meinhart CD, et al. Dielectrophoretic separation of platelets from diluted whole blood in microfluidic channels. Electrophoresis. 2008; 29(6):1213–8. Epub 2008/02/22. [PubMed: 18288670]
13. Pethig R, Menachery A, Pells S, De Sousa P. Dielectrophoresis: a review of applications for stem cell research. Journal of biomedicine & biotechnology. 2010; 2010:182581. Epub 2010/05/22. [PubMed: 20490279]
14. Flanagan LA, Lu J, Wang L, Marchenko SA, Jeon NL, Lee AP, et al. Unique dielectric properties distinguish stem cells and their differentiated progeny. Stem cells. 2008; 26(3):656–65. [PubMed: 18096719]
15. Labeed FH, Lu J, Mulhall HJ, Marchenko SA, Hoettges KF, Estrada LC, et al. Biophysical characteristics reveal neural stem cell differentiation potential. PloS one. 2011; 6(9):e25458. Epub 2011/10/08. [PubMed: 21980464]
16. Bagnaninchi PO, Drummond N. Real-time label-free monitoring of adipose-derived stem cell differentiation with electric cell-substrate impedance sensing. Proc Natl Acad Sci USA. 2011; 108(16):6462–7. [PubMed: 21464296]
17. Vykoukal DM, Gascoyne PR, Vykoukal J. Dielectric characterization of complete mononuclear and polymorphonuclear blood cell subpopulations for label-free discrimination. Integrative biology : quantitative biosciences from nano to macro. 2009; 1(7):477–84. Epub 2009/12/22. [PubMed: 20023758]
18. Gagnon ZR. Cellular dielectrophoresis: applications to the characterization, manipulation, separation and patterning of cells. Electrophoresis. 2011; 32(18):2466–87. Epub 2011/09/17. [PubMed: 21922493]
19. Talary MS, Mills KI, Hoy T, Burnett AK, Pethig R. Dielectrophoretic separation and enrichment of CD34+ cell subpopulation from bone marrow and peripheral blood stem cells. Med Biol Eng Comput. 1995; 33(2):235–7. [PubMed: 7543968]
20. Vykoukal J, Vykoukal DM, Freyberg S, Alt EU, Gascoyne PRC. Enrichment of putative stem cells from adipose tissue using dielectrophoretic field-flow fractionation. Lab on a chip. 2008; 8(8): 1386–93. [PubMed: 18651083]

21. Stephens M, Talary MS, Pethig R, Burnett AK, Mills KI. The dielectrophoresis enrichment of CD34+ cells from peripheral blood stem cell harvests. Bone Marrow Transplant. 1996; 18(4):777–82. [PubMed: 8899194]
22. Altomare L, Borgatti M, Medoro G, Manaresi N, Tartagni M, Guerrieri R, et al. Levitation and movement of human tumor cells using a printed circuit board device based on software-controlled dielectrophoresis. Biotechnology and bioengineering. 2003; 82(4):474–9. [PubMed: 12632404]
23. Becker FF, Wang XB, Huang Y, Pethig R, Vykoukal J, Gascoyne PR. The removal of human leukaemia cells from blood using interdigitated microelectrodes. J Phys D: Appl Phys. 1994; 27(12):2659–62.
24. Wang X, Yang J, Gascoyne PR. Role of peroxide in AC electrical field exposure effects on friend murine erythroleukemia cells during dielectrophoretic manipulations. Biochim Biophys Acta. 1999; 1426(1):53–68. [PubMed: 9878687]
25. Menachery A, Pethig R. Controlling cell destruction using dielectrophoretic forces. IEE Proceedings-Nanobiotechnology. 2005; 152(4):145–9. [PubMed: 16441171]
26. Huang Y, Joo S, Duhon M, Heller M, Wallace B, Xu X. Dielectrophoretic cell separation and gene expression profiling on microelectronic chip arrays. Analytical chemistry. 2002; 74(14):3362–71. [PubMed: 12139041]
27. Docoslis A, Kalogerakis N, Behie L. Dielectrophoretic forces can be safely used to retain viable cells in perfusion cultures of animal cells. Cytotechnology. 1999; 30(1):133–42. [PubMed: 19003362]
28. Desai SP, Voldman J. Cell-based sensors for quantifying the physiological impact of microsystems. Integr Biol. 2011; 3(1):48–56. Epub 2010/10/16.
29. Prieto JL, Lu J, Nourse JL, Flanagan LA, Lee AP. Frequency discretization in dielectrophoretic assisted cell sorting arrays to isolate neural cells. Lab on a chip. 2012; 12(12):2182–9. Epub 2012/03/31. [PubMed: 22460949]
30. Wang L, Lu J, Marchenko SA, Monuki ES, Flanagan LA, Lee AP. Dual frequency dielectrophoresis with interdigitated sidewall electrodes for microfluidic flow-through separation of beads and cells. Electrophoresis. 2009; 30(5):782–91. [PubMed: 19197906]
31. Flanagan LA, Rebaza LM, Derzic S, Schwartz PH, Monuki ES. Regulation of human neural precursor cells by laminin and integrins. Journal of neuroscience research. 2006; 83(5):845–56. [PubMed: 16477652]
32. Jayat C, Ratinaud MH. Cell cycle analysis by flow cytometry: principles and applications. Biol Cell. 1993; 78(1–2):15–25. Epub 1993/01/01. [PubMed: 8220224]
33. Kirson ED, Dbaly V, Tovarys F, Vymazal J, Soustiel JF, Itzhaki A, et al. Alternating electric fields arrest cell proliferation in animal tumor models and human brain tumors. Proc Natl Acad Sci USA. 2007; 104(24):10152–7. [PubMed: 17551011]
34. Goldman S. Glia as neural progenitor cells. Trends Neurosci. 2003; 26(11):590–6. [PubMed: 14585598]
35. Grosse C, Schwan H. Cellular membrane potentials induced by alternating fields. Biophysical Journal. 1992; 63(6):1632–42. [PubMed: 19431866]
36. Pistollato F, Chen H-L, Schwartz PH, Basso G, Panchision DM. Oxygen tension controls the expansion of human CNS precursors and the generation of astrocytes and oligodendrocytes. Mol Cell Neurosci. 2007; 35(3):424–35. [PubMed: 17498968]
37. Heida T, Rutten WL, Marani E. Experimental investigation on neural cell survival after dielectrophoretic trapping. Arch Physiol Biochem. 2002; 110(5):373–82. [PubMed: 12530622]
38. Heida T, Vulto P, Rutten WL, Marani E. Viability of dielectrophoretically trapped neural cortical cells in culture. J Neurosci Methods. 2001; 110(1–2):37–44. [PubMed: 11564523]
39. Puttaswamy SV, Sivashankar S, Chen RJ, Chin CK, Chang HY, Liu CH. Enhanced cell viability and cell adhesion using low conductivity medium for negative dielectrophoretic cell patterning. Biotechnology journal. 2010; 5(10):1005–15. Epub 2010/10/12. [PubMed: 20931598]
40. Gascoyne PR, Vykoukal J. Dielectrophoresis-based sample handling in general-purpose programmable diagnostic instruments. Proceedings of the IEEE. 2004; 92(1):22–42. [PubMed: 19684877]

41. Konig S, Hinard V, Arnaudeau S, Holzer N, Potter G, Bader CR, et al. Membrane hyperpolarization triggers myogenin and myocyte enhancer factor-2 expression during human myoblast differentiation. The Journal of biological chemistry. 2004; 279(27):28187–96. Epub 2004/04/16. [PubMed: 15084602]

42. Shirihai O, Attali B, Dagan D, Merchav S. Expression of two inward rectifier potassium channels is essential for differentiation of primitive human hematopoietic progenitor cells. J Cell Physiol. 1998; 177(2):197–205. Epub 1998/10/10. [PubMed: 9766516]

43. Yamada M, Tanemura K, Okada S, Iwanami A, Nakamura M, Mizuno H, et al. Electrical stimulation modulates fate determination of differentiating embryonic stem cells. Stem cells. 2007; 25(3):562–70. Epub 2006/11/18. [PubMed: 17110622]

44. Hoettges KF. Dielectrophoresis as a cell characterisation tool. Methods Mol Biol. 2010; 583:183–98. Epub 2009/09/19. [PubMed: 19763465]

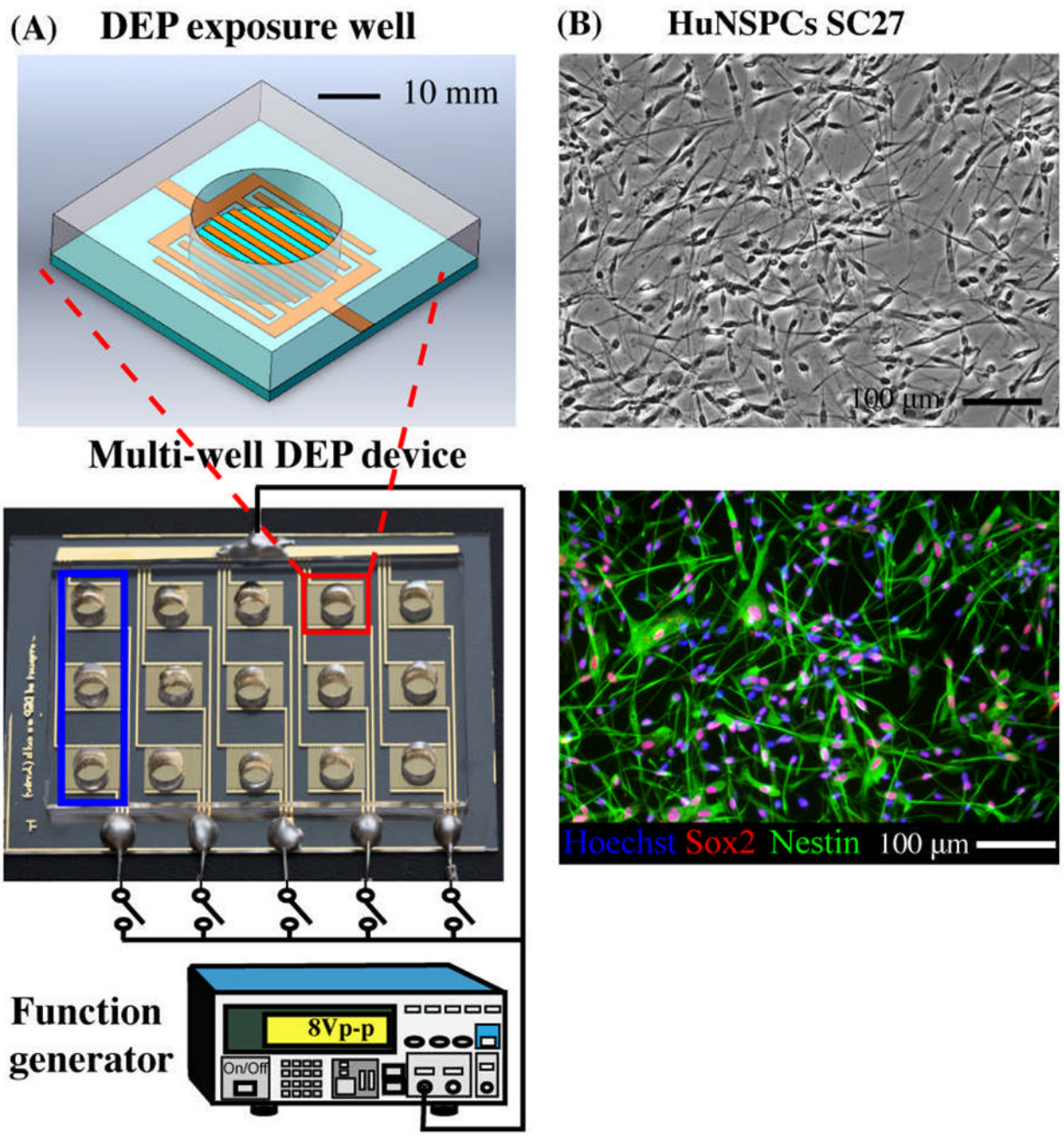

Fig. 1. Multi-well device and experimental setup for testing effects of DEP force on NSPCs

(A) DEP exposure well (top schematic) contains interdigitated gold-plated electrodes at the bottom of the well (sides of well are PDMS). Fifteen individual wells (red square) make up the multi-well DEP device (bottom schematic), which is connected to a function generator to energize the electrodes (energized by $8V_{peak\text{-}peak}$). The bottom electrical head serves as a DEP force switch for each group of three exposure wells (blue square). The symbol, ⟜, represents a switch in the circuit. ***(B)*** Undifferentiated HuNSPCs (SC27) are grown as adherent cultures (phase contrast panel) and express the neural stem cell markers Sox2 and Nestin (fluorescence panel, 98.0 +/− 0.5% of the cells express either Sox2 or Nestin and 78.6 +/− 2.7% co-express both markers, N=1300 cells). All cell nuclei are stained with

Hoechst. NSPCs are grown as adherent cultures but were dissociated to form a cell suspension for all DEP exposure experiments. Data are represented as mean ± SE.

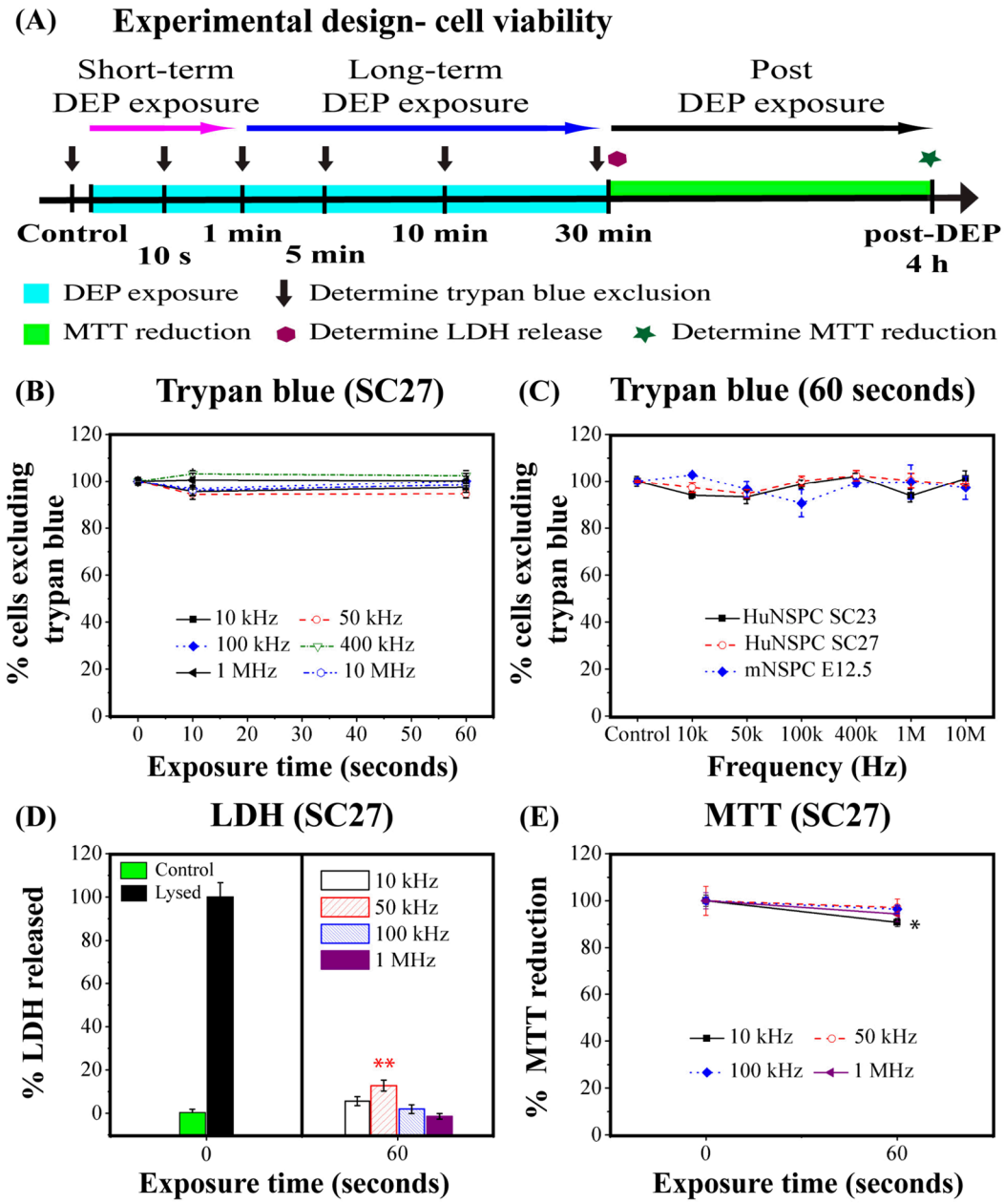

Fig. 2. Short-term DEP exposure has negligible effects on NSPC survival

(A) Schematic of experimental design to test effects of short-term and long-term DEP exposure on cell survival. ***(B)*** HuNSPCs exposed to DEP frequencies for 0, 10, or 60 sec exhibit no significant decrease in cell survival as determined by trypan blue exclusion. ***(C)*** The cell survival of three different sets of NSPCs (HuNSPCs SC23 or SC27 and mNSPCs E12.5) is not affected by 60 sec DEP exposure at any frequency. ***(D)*** Left panel: The baseline level of LDH released by intact control HuNSPCs (SC27 cells in DEP buffer not exposed to DEP force) is set as 0%. The maximum amount of LDH release is shown for HuNSPCs (SC27) lysed with triton-X100 and is set as 100% LDH released. Right panel: Release of LDH by cells after 60 sec exposure to DEP frequencies is only above background levels at 50 kHz. ***(E)*** The cellular metabolic activity of HuNSPCs (SC27) after 60 sec

exposure to DEP frequencies remains greater than 90% for all conditions. Data are represented as mean ± SE (*, p-value < 0.05 and **, p-value <0.01).

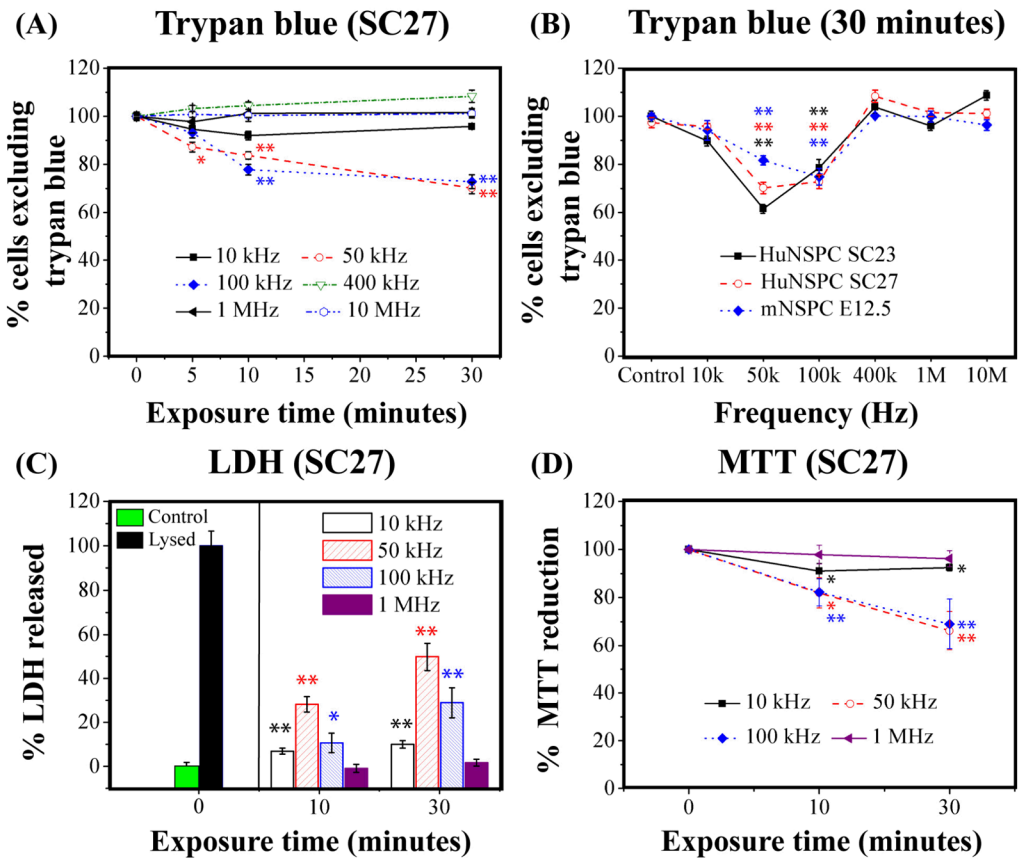

Fig. 3. Long-term DEP exposure to frequencies of 50 kHz and 100 kHz, but not lower or higher frequencies, decreases cell survival

(A) Survival of HuNSPCs (SC27) as determined by trypan blue exclusion after DEP exposure is most affected by 50 and 100 kHz frequencies. *(B)* The cell survival of three different sets of NSPCs (SC23 or SC27 HuNSPCs and E12.5 mNSPCs) is decreased after 30 min exposure to DEP frequencies of 50 kHz and 100 kHz, but not other frequencies. *(C)* Left panel: Amount of LDH released by control cells (in DEP buffer but not exposed to DEP force) is set as 0% LDH release and amount of LDH released by cells that were completely lysed with triton-X100 is set as 100% LDH release. Right panel: Release of LDH by cells after exposure to DEP frequencies is greatest at 50 kHz. *(D)* Cellular metabolic activity was decreased primarily by long-term DEP exposure to frequencies of 50 and 100 kHz. Data are represented as mean ± SE (*, *p*-value < 0.05 and **, *p*-value <0.01).

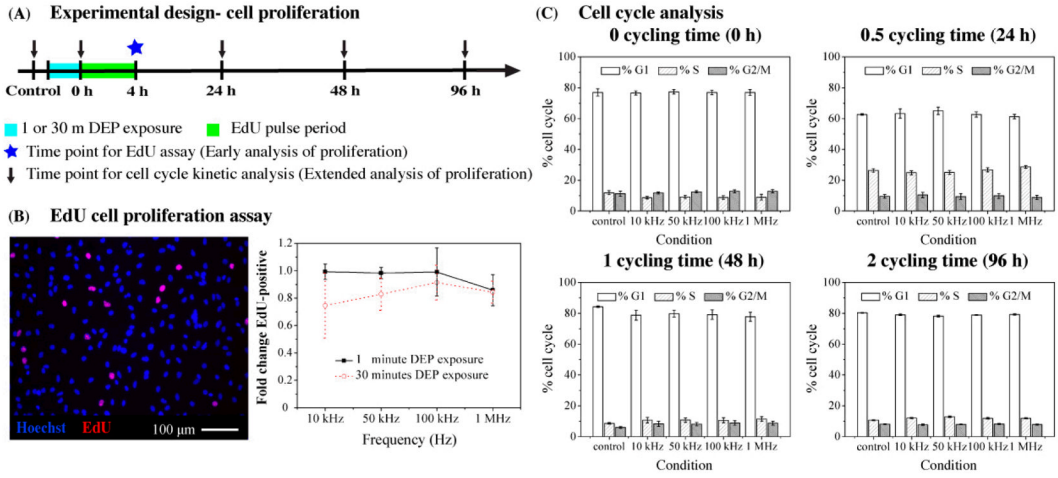

Fig. 4. DEP exposure does not alter NSPC proliferation

(A) Schematic depicts the experimental design to test the effects of DEP on cell proliferation. ***(B)*** Left panel: Image of untreated HuNSPCs (SC27) demonstrates that 5–10 % of the cells are EdU-positive (red). All nuclei are stained blue. Right panel: No significant difference in cell division as measured by EdU incorporation was observed after DEP exposure for 1 or 30 min at all frequencies tested. ***(C)*** Control cells and those exposed to various DEP frequencies did not significantly differ in cell cycle kinetics. Cells were analyzed immediately after DEP exposure and at various times to allow up to 2 cell cycles to occur (~48 h doubling time). Data are represented as mean ± SE.

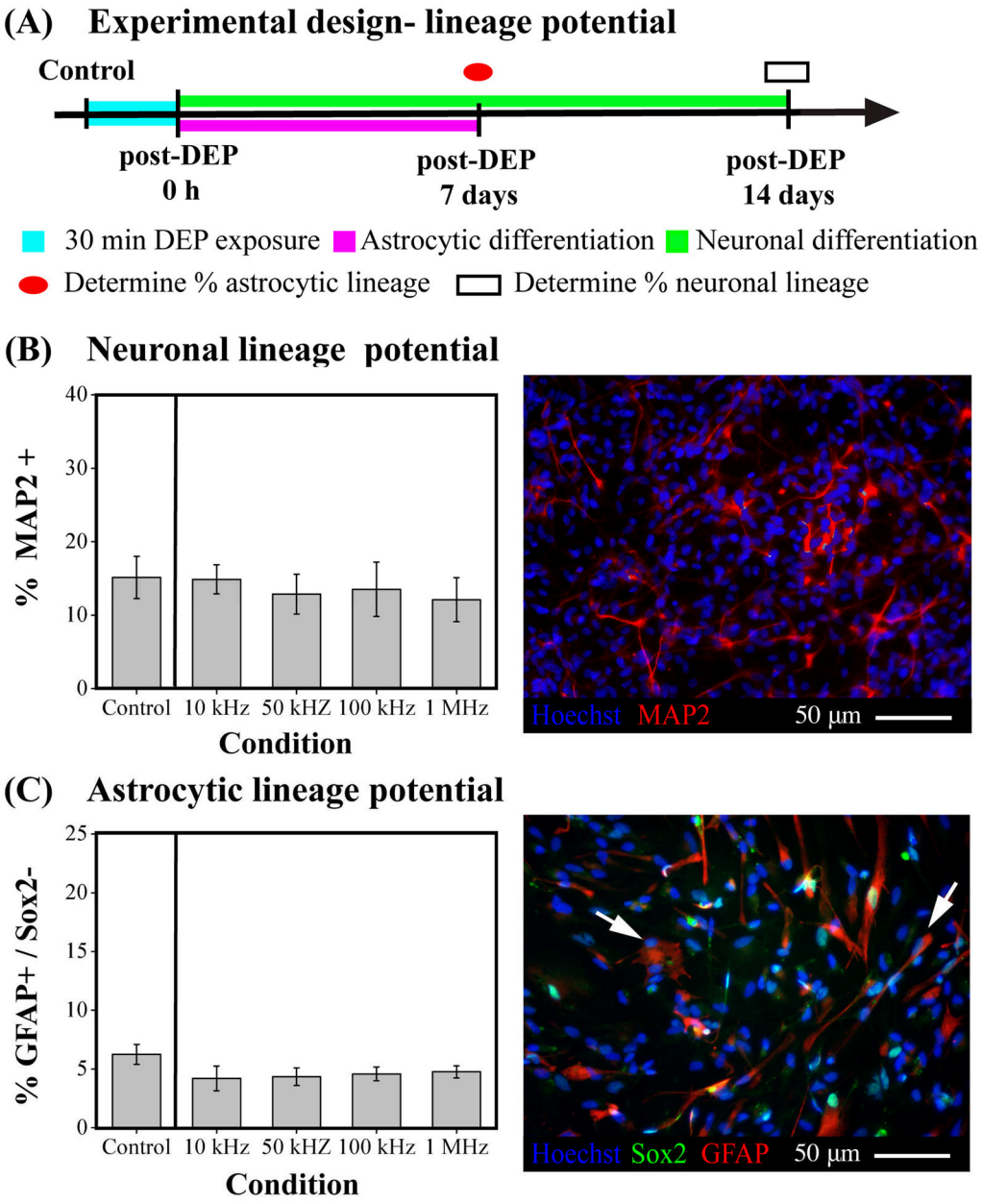

Fig. 5. DEP exposure does not interfere with differentiation of NSPCs into neuronal and astrocytic lineages

(A) Schematic portrays the experimental design to test effects of DEP on neuronal and astrocytic lineage potential of NSPCs. ***(B)*** Left panel: The neuronal lineage potential of SC27 HuNSPCs (as shown by generation of MAP2+ cells) is not altered by long-term DEP exposure at various DEP frequencies. Control cells were not exposed to DEP force. Right panel: Image shows HuNSPCs (SC27) differentiated for 14 days and stained with MAP2 antibody (red) to detect neurons. All nuclei are stained blue. ***(C)*** Left panel: The astrocytic lineage potential of SC27 HuNSPCs (as shown by generation of GFAP+/Sox2− cells) is not modified by long-term DEP exposure at various DEP frequencies. Right panel: Image shows HuNSPCs (SC27) differentiated for 7 days and co-stained with GFAP (red) and Sox2

(green) antibodies (GFAP+/Sox2− astrocytes are shown by arrows). All nuclei are stained blue. Data are represented as mean ± SE.

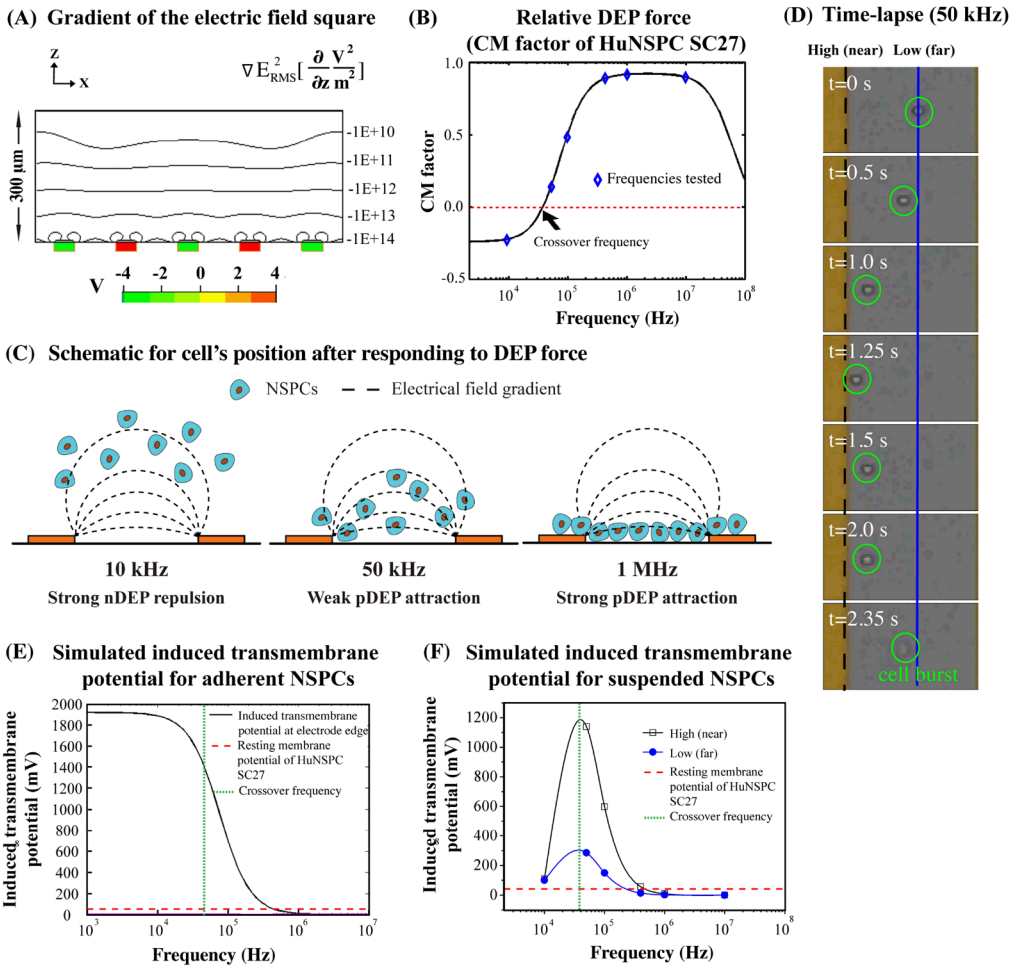

Fig. 6. Rapid increases in the transmembrane potential of cells at frequencies slightly above the crossover frequency cause membrane disruption of NSPCs in suspension

(A) The iso-curves represent the root mean square of the gradient of the electric field square in the z direction (see equation above graph). The induced DEP force is proportional to the iso-curve value. The red and green boxes represent electrodes with either positive or negative applied voltages. *(B)* Graph shows the simulated CM factor (parameters in Table S1 in Supporting Material) of HuNSPCs (SC27) at various frequencies. The blue diamonds represent the CM factor of SC27 cells at frequencies used in the current study to test the toxicity of DEP exposure to cells. The derived crossover frequency of SC27 cells is 45 kHz (red dashed line). *(C)* Schematic represents cells' final positions relative to electrodes at various applied frequencies. *(D)* Time lapse images show behavior of a cell (circled in green) in response to 50 kHz DEP frequency over ~2.4 sec. The dashed black line represents the edge of the electrode (high electric field) while the solid blue line denotes the position of cells that have moved away from the electrode (lower electric field). *(E)* The graph shows the induced transmembrane potential of a hypothetical population of adherent SC27 cells at the edge of electrodes. The lower the frequency applied, the higher the induced transmembrane potential of NSPCs. The red dashed line represents the resting membrane potential of SC27 HuNSPCs, 51.6+/−2.6 mV, n=20. The green dashed line represents the crossover frequency of SC27 cells (~45 kHz). The parameters for the modeling are listed in Table S1 in Supporting Material. *(F)* The graph depicts the frequency-dependent induced transmembrane potential of suspended SC27 cells accounting for the final position of the

cells relative to the electrode (and thus the strength of the electric field). The black line denotes the induced transmembrane potential for cells in a region of high electric field near the electrodes, as shown by the black dashed line in D, and the blue line denotes the induced transmembrane potential for cells in a region of low electric field farther from the electrodes, as shown by the blue line in D. The parameters for the modeling are listed in Table S1 in Supporting Material.

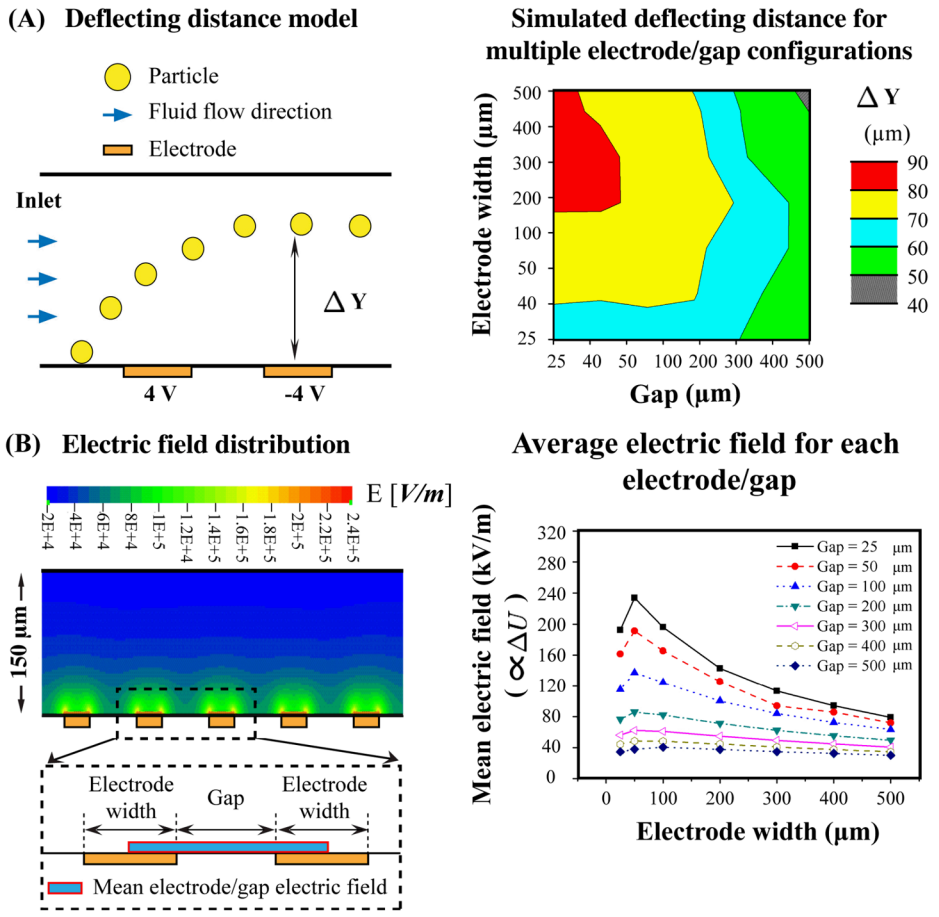

Fig. 7. Electrode and gap size optimization for maximal cell deflection and minimal electric field exposure

(A) The left panel schematic depicts an example of the CFD modeling used to determine the deflection of a particle in response to the DEP electric field from a pair of interdigitated electrodes set to 8V $_{peak\text{-}peak}$. Particles and fluid enter the channel from the left and as the particle passes by the electrode and gap it is deflected upon encountering the electric field. Delta Y represents the distance the particle moved due to the induced DEP force. The right panel color surface plot shows delta Y as a function of the sizes of the electrodes and the gaps between them. ***(B)*** The left panel shows a color plot of the electric field distribution above the electrodes for a 50 μm electrode × 100 μm gap configuration. One pair of electrodes with intervening gap is enlarged in the dashed box to demonstrate the area used to calculate the mean electric field for each electrode/gap (blue and red box), which is graphed in the right panel. The right panel graph portrays the mean electric field, which is proportional to the induced transmembrane potential (ΔU), for multiple electrode and gap sizes and combinations.